Characterization of rarefaction waves in van der Waals fluids

Albert Yuen and John J. Barnard

Phys. Rev. E **92**, 062307 — Published 18 December 2015

DOI: 10.1103/PhysRevE.92.062307

Characterization of Rarefaction Waves in Van Der Waals Fluids

Albert Yuen*
Department of Nuclear Engineering, University of California, Berkeley, CA 94720, USA
Department of Physics, University of California, Berkeley, CA 94720, USA and
Lawrence Berkeley National Laboratory, Berkeley, CA 94720, USA

John J. Barnard†
Lawrence Livermore National Laboratory, Livermore, CA 94550, USA

We calculate the isentropic evolution of an instantaneously heated foil, assuming a van der Waals equation of state with the *Maxwell construction*. The analysis by Yuen and Barnard [Phys. Rev. E **92**, 033019 (2015)] is extended for the particular case of three degrees of freedom. We assume heating to temperatures in the vicinity of the critical point. The self-similar profiles of the rarefaction waves describing the evolution of the foil display plateaus in density and temperature due to a phase transition from the single phase to the two-phase regime. The hydrodynamic equations are expressed in a dimensionless form and the solutions form a set of universal curves, depending on a single parameter: the dimensionless initial entropy. We characterize the rarefaction waves by calculating how the plateau length, density, pressure, temperature, velocity, internal energy and sound speed vary with dimensionless initial entropy.

I. INTRODUCTION

The Warm Dense Matter (WDM) regime is reached when the density and the temperature are approximately in the range of 0.1 to 10 times the solid density, and 0.01 eV to 10 eV, extended up to 50 eV by some authors[1, 2]. WDM conditions can occur naturally [3] or artificially, e.g., by heating thin foils with intense lasers[3–5] or ion beams[5–8]. When the heating time is much shorter than the hydrodynamic time and the energy deposition is volumetric, the foils can be assumed first to be uniformly and instantaneously heated, and then to expand from a high temperature solid or liquid state to a lower temperature vapor state. We focus our study near the critical point - the point beyond which there is no distinction between phases. The boundary between the vapor phase and the liquid phase as a function of density and temperature is still under investigation for many materials, such as refractory metals[9], and, for some materials, is in the WDM regime.

In previous experiments under similar settings, constant density plateaus had been inferred theoretically[10–15]. In Ref. [16], such plateaus of constant density (and pressure, temperature, energy density, velocity) during the phase transition from a single-phase to the two-phase regime are found in van der Waals (VDW) fluids with an arbitrary number of degrees of freedom. In the present paper, we extend the semi-analytical formalism of Ref. [16] for the specific case of a VDW equation of state (EOS) with three degrees of freedom supplemented with the *Maxwell construction*: we use Riemann's solution[17, 18] in 1D to describe the dynamics of the heated target, modeled by a semi-infinite slab of material that initially extends from $z = -\infty$ to $z = 0$. This effectively restricts the scope of this paper to the early stage of the foil expansion before the rarefaction waves from both sides of a given thin foil meet, coined as the *simple wave regime* in Ref. [19]. In addition to its mathematical simplicity, the chosen EOS displays two-phase behavior, and has successfully modeled various real condensed matter systems qualitatively, e.g. the structure and properties of molecular liquids, liquid metals and crystals, their freezing and melting, and their critical behaviors[20]. With three degrees of freedom, the VDW EOS also corresponds to a monatomic gas at low density and does not yield rarefaction shockwaves[16, 18, 21–23]. Nevertheless, the quantitative application of the VDW EOS must be checked and several directly measurable quantities can help us confirm, improve or reject the VDW model.

The solutions of our model equations form a set of universal curves, depending on a single parameter: the dimensionless initial entropy. We characterizes the evolution of plateaus for various initial entropies, and our semi-analytic results are numerically tested against the 1D planar Lagrangian hydrodynamic code DISH[24]. These studies are useful for developing a qualitative understanding of heated foils expanding through a phase change, as well as for benchmarking codes that encompass more realistic EOS. In order to make a concrete connection to the physical values of density and temperature, we describe an algorithm in Appendix A that links the dimensionless quantities characterizing the rarefaction waves (e.g., the length of plateaus and ratios of initial density to plateau density) to physical variables.

* albert.yuen@berkeley.edu
† barnard1@llnl.gov

II. HYDRODYNAMICS OF THE VAN DER WAALS FLUID

A. Equation of state: the Van der Waals model

The fluid is modeled by the VDW EOS with three degrees of freedom[25], in contrast to the arbitrary number of degrees of freedom in Ref. [16], meaning that only the rarefaction waves of case 3 and 6 of Ref. [16] out of the eight possible cases will be encountered:

$$p = \frac{\rho k T}{A m_{\rm amu}(1-b\rho)} - a\rho^2, \tag{1a}$$

$$s = \frac{k}{A m_{\rm amu}} \ln\left(A m_{\rm amu} \frac{1-b\rho}{\rho \lambda^3} \right), \tag{1b}$$

$$c_s^2 = \left.\frac{\partial p}{\partial \rho}\right|_s = \frac{5}{3}\frac{kT}{A m_{amu}}\frac{1}{(1-b\rho)^2} - 2a\rho, \tag{1c}$$

$$\epsilon = \frac{3}{2}\frac{kT}{A m_{amu}} - a\rho, \tag{1d}$$

where p, ρ, T, s and c_s are respectively the pressure, density, temperature, entropy and sound speed of the fluid. A is the mass number of the atomic species of the fluid, k the Boltzmann constant, m_{amu} the atomic mass unit. $\lambda = h/(2\pi A m_{\rm amu} kT)^{1/2}$ is the de Broglie wavelength. a and b are the VDW constants of the EOS[26, 27]. Following Ref. [16], the problem is treated more generally by scaling all quantities by the critical or characteristic parameters of a given material under investigation, and are denoted with a tilde $\tilde{}$ (e.g $\tilde{\rho}$). The critical density ρ_c, pressure p_c and temperature T_c are

$$\rho_c = \frac{1}{3b}, \quad p_c = \frac{1}{27}\frac{a}{b^2} \quad \text{and} \quad \frac{kT_c}{A m_{amu}} = \frac{8}{27}\frac{a}{b}, \tag{2}$$

and the characteristic sound speed, energy density and entropy are $c_{s,0}^2 = p_c/\rho_c$, $\epsilon_c = \epsilon(\rho_c, T_c) = a/(9b)$ and $s_c = s(\rho_c, T_c)$.

From Eqs. (1) and (2), the dimensionless VDW equations yield

$$\tilde{p} = \frac{p}{p_c} = 8\frac{\tilde{\rho}\tilde{T}}{3-\tilde{\rho}} - 3\tilde{\rho}^2, \tag{3a}$$

$$\tilde{s} = \frac{s - s_c}{k/(A m_{\rm amu})} = \ln\left(\frac{3-\tilde{\rho}}{2\tilde{\rho}} \tilde{T}^{3/2} \right), \tag{3b}$$

$$\tilde{c}_s^2 = \frac{c_s^2}{c_{s,0}^2} = 40\frac{\tilde{T}}{(3-\tilde{\rho})^2} - 6\tilde{\rho}, \tag{3c}$$

$$\tilde{\epsilon} = \frac{\epsilon}{\epsilon_c} = 4\tilde{T} - 3\tilde{\rho}. \tag{3d}$$

For isotherms $\tilde{T} < 1$, the regime of hydrodynamical instability where $\partial\tilde{p}/\partial\tilde{\rho}|_{\tilde{T}} < 0$ is assumed to be in equilibrium state using the *Maxwell construction*[28].

B. Hydrodynamics and dimensionless solutions

In Ref. [16], and following Ref. [17, 18], assuming a neutral and non-viscous fluid without mass source or sink, it was shown that the equations governing the dynamics of a 1D Eulerian fluid in Cartesian coordinates at time t and axial coordinate z can be transformed using the self-similar variable $\xi = z/t$ and the relevant asymptotic conditions. Scaled by the characteristic parameters, this yields the dimensionless hydrodynamical equation

$$\tilde{\xi}(\tilde{\rho}) = -\tilde{I}(\tilde{\rho}) - \tilde{c_s}(\tilde{\rho}). \tag{4}$$

Here, $\tilde{\xi}(\tilde{\rho}) = \xi(\rho)/c_{s,0}$, $\tilde{I}(\tilde{\rho}) = I(\rho)/c_{s,0}$ and $\tilde{c_s}(\tilde{\rho}) = c_s(\rho)/c_{s,0}$ where $I(\rho) = \int_{\rho_0}^{\rho} \frac{c_s(\rho')}{\rho'}\,\mathrm{d}\rho'$. Eq. (4) is solved for the isentropes $\tilde{s}_0 = -2$, -1, 0, 1 and 2 at initial density $\tilde{\rho} = 2.7$. Following Eq. (3b), this is equivalent to initial temperatures $\tilde{T}_0 = 1.8$, 3.5, 6.8, 13 and 26. These isentropes in the $(\tilde{\rho}, \tilde{T})$ diagram are displayed in Fig. 1. We can distinguish two types of rarefaction waves: If $\tilde{s}_0 \leq 0$, the fluid enters the two-phase regime from a liquid state (referred as case 3 in Ref. [16]). If $\tilde{s}_0 \geq 0$, the fluid enters the two-phase regime from a gaseous state (referred as case 6 in Ref. [16]). The density, pressure, temperature, fluid velocity, fluid mass energy and sound speed profiles as a function of $\tilde{\xi}$ are solved semi-analytically using Mathematica[29] and compared numerically against the 1D planar Lagrangian hydrodynamic code DISH[24]. The semi-analytical and numerical results almost perfectly overlap, and are plotted in Fig. 2 (with an expanded version in Fig. 3). Except for the sound speed profile, the profiles display plateaus whose length are ex-

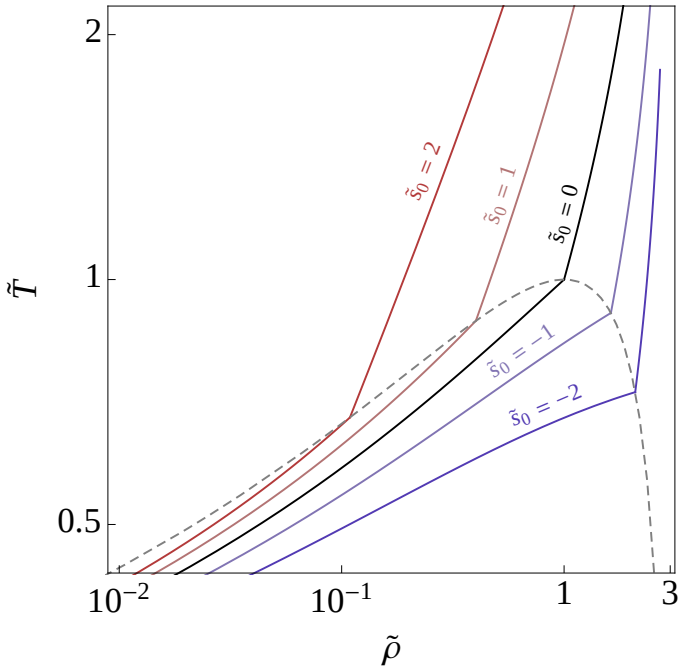

FIG. 1. (Color online) $(\tilde{\rho}, \tilde{T})$ diagram of isentropic expansions. The grey dashed curve represents the Maxwell-constructed binodal. The full lines are isentropes, all starting from $\tilde{\rho} = 2.7$ and initial temperature $\tilde{T}_0 = 1.8$, 3.5, 6.8, 13 and 26, representing entropies $\tilde{s}_0 = -2$ (dark blue), -1 (light blue), 0 (black), 1 (light brown) and 2 (dark brown).

clusively function of the $\tilde{s}_0$. This is not surprising as the plateaus arise precisely because of the discontinuity of the sound speed between its value $\tilde{c}^+_{s,b} = \tilde{c}_s(\tilde{\rho}^+_b)$ at the vicinity of the binodal in the single-phase regime and $\tilde{c}^-_{s,b} = \tilde{c}_s(\tilde{\rho}^-_b)$ at the vicinity of the binodal in the two-phase regime. Here, the variables with subscript "b" are their values at the binodal. This discontinuity is due to the *Maxwell construction* ($\partial\tilde{p}/\partial\tilde{\rho}|_{\tilde{T}}$ is no longer a smooth function of $\tilde{\rho}$ at $\tilde{\rho} = \tilde{\rho}_b$) and, from Eq. (4), yields $\Delta\tilde{\xi}_b = \tilde{c}^+_{s,b} - \tilde{c}^-_{s,b}$. A graphical depiction of the discontinuity of the sound speed as a function of $\tilde{s}_0$ is shown in Fig. 4. An interesting feature of the isentropic curves in Figs. 2 and 3 is the sole dependency of the shape of these curves on $\tilde{s}_0$, and that, in addition to this property, the values of the parameters at the binodal draw a continuous function of $\tilde{s}_0$ (except for $\tilde{c}_s$, as previously mentioned), as shown in Fig. 5. This property can also be graphically observed in the ($\tilde{\rho}$,$\tilde{T}$) diagram in Fig. 1 when isentropic curves cross the Maxwell-constructed binodal: increasing the initial dimensionless entropy $\tilde{s}_0$ from a negative value means that, at the interception point, the density $\tilde{\rho}_b$ decreases and the temperature $\tilde{T}_b$, at first, increase. These trends continue until $\tilde{s}_0 = 0$ is reached, i.e. at the critical point. Further increasing $\tilde{s}_0$ further decreases $\tilde{\rho}_b$ but now also decreases $\tilde{T}_b$ along the binodal. The evolution of the pressure at the binodal $\tilde{p}_b$ parameterized by $\tilde{s}_0$ is similar to the evolution of $\tilde{T}_b$, also with a maximum occurring at the critical point. The internal energy density $\tilde{\epsilon}_b$, which includes a potential energy term in addition to the kinetic energy (temperature) term, maximizes at higher entropy than $\tilde{s}_0 = 0$, i.e. lower density than the critical density $\tilde{\rho} = 1$. The velocity at the binodal $\tilde{v}_b$ (and hence the velocity of the plateau region when it exists) monotonically increases as $\tilde{s}_0$ increases. The length of the plateau $\Delta\tilde{\xi}_b$ monotonically decreases to 0 with increasing $\tilde{s}_0$. Heuristically, the sound speed in the single phase at the vicinity of the binodal, denoted $\tilde{c}^+_{s,b}$, gets larger as $\tilde{s}_0$ decreases (getting closer to the $\tilde{\rho} = 3$ limit which represents the upper limit of the density for a VDW fluid) whereas the sound speed in the two phase regime at the vicinity of the binodal, denoted $\tilde{c}^-_{s,b}$, gets smaller, since the isobars are flatter, and the isentropic curves are relatively shallow. The difference in sound speed should be greatest at low entropy (as can be seen from fig. 5), and therefore $\Delta\tilde{\xi}_b$ should decrease with increasing $\tilde{s}_0$, meaning the widest plateaus $\Delta\tilde{\xi}_b$ will be observed at the lowest initial entropy.

III. DISCUSSION

This analysis is applicable to any VDW fluid (here, with $f = 3$ degrees of freedom) as the solutions can be scaled back to dimensional quantities using the appropriate A, a and b that characterize a given chemical element. While all equations of state yield a self-similar profile, only "cubic" EOS, i.e. when the density expressed as a function of pressure and temperature is the solution of a cubic equation in ρ , yield a single set of dimensionless curves that depends on only one free parameter, here the initial dimensionless entropy $\tilde{s}_0$. A similar characterization of trends could be carried out for any specific value of f.

While such a complete solution set to the problem should not necessarily be directly applied to any real specific material, this can lead to insights that are not obtainable when non-idealizations are included in the problem (e.g. ionizations or geometrical effects). Qualitative trends - e.g., higher initial temperatures results in shorter plateau regions - can be obtained from our model. This analysis also allows benchmarking multi-dimensional fluid codes with more elaborate (but sometimes less intuitive) EOS. We emphasize that our method of obtaining the initial and critical parameters, should be used for determining the parameters to be used in the model when comparing with any real material, but not necessarily as an absolute way of inferring the critical point in a particular experiment.

In addition, certain physical quantities can be obtained directly from these measurements, independent of the assumed EOS. For example, $\Delta\xi_b = \Delta c_{s,b}$ where $\Delta c_{s,b} = c_s(\rho^+_b) - c_s(\rho^-_b)$ is the difference between the sound speed in the single phase and in the two-phase regime at the vicinity of the binodal. Similarly, measuring the extent of $\tilde{\xi}$ in the single phase, $\xi(\rho^+_b) - \xi(\rho_0) = c_s(\rho_0) - c_s(\rho^+_b) + \int_{\rho_0}^{\rho_b} c_s(\rho')/\rho' \, \mathrm{d}\rho'$, gives some indirect information about the sound speed in the single phase. Measurements of ρ_b directly for various initial temperatures allows one to map out the binodal and find the critical density ρ_c (e.g., at the maximum of ρ_b versus initial temperature). Also, as shown in Ref.[30], the sound speed as a function of position and density can be inferred from a line integral of the density from a position z_0 with a known sound speed $c_s(\rho_0)$ to a particular point z in question as $c_s = -(\int_{z_0}^{z} \rho \, \mathrm{d}z)/(\rho t) + \rho_0 c_s(\rho_0)/\rho$. Note that the presence of plateaus in density indicates that there are discontinuities in the sound speed so care must be taken so that integrations are not done across discontinuities. From $p(z) = p_0 + \int_{z_0}^{z} c_s^2(\partial p/\partial z) \, \mathrm{d}z$ where z_0 is a position with a known sound speed and pressure, the pressure is thus directly inferred on an isentrope (assuming the data is precise enough to compute the integrals).

It is hoped that having specific solutions to the hydrodynamic equations for a specific EOS will lend to a greater understanding of the behaviors of expanding foils with a more complex EOS.

ACKNOWLEDGMENTS

The authors are pleased to acknowledge numerous valuable discussions with R. M. More, E. Startsev and I. Kaganovich. This work was performed under the auspices of the U.S. Department of Energy by Lawrence Livermore National Security, LLC, Lawrence Livermore National Laboratory under Contract DE-AC52-07NA27344

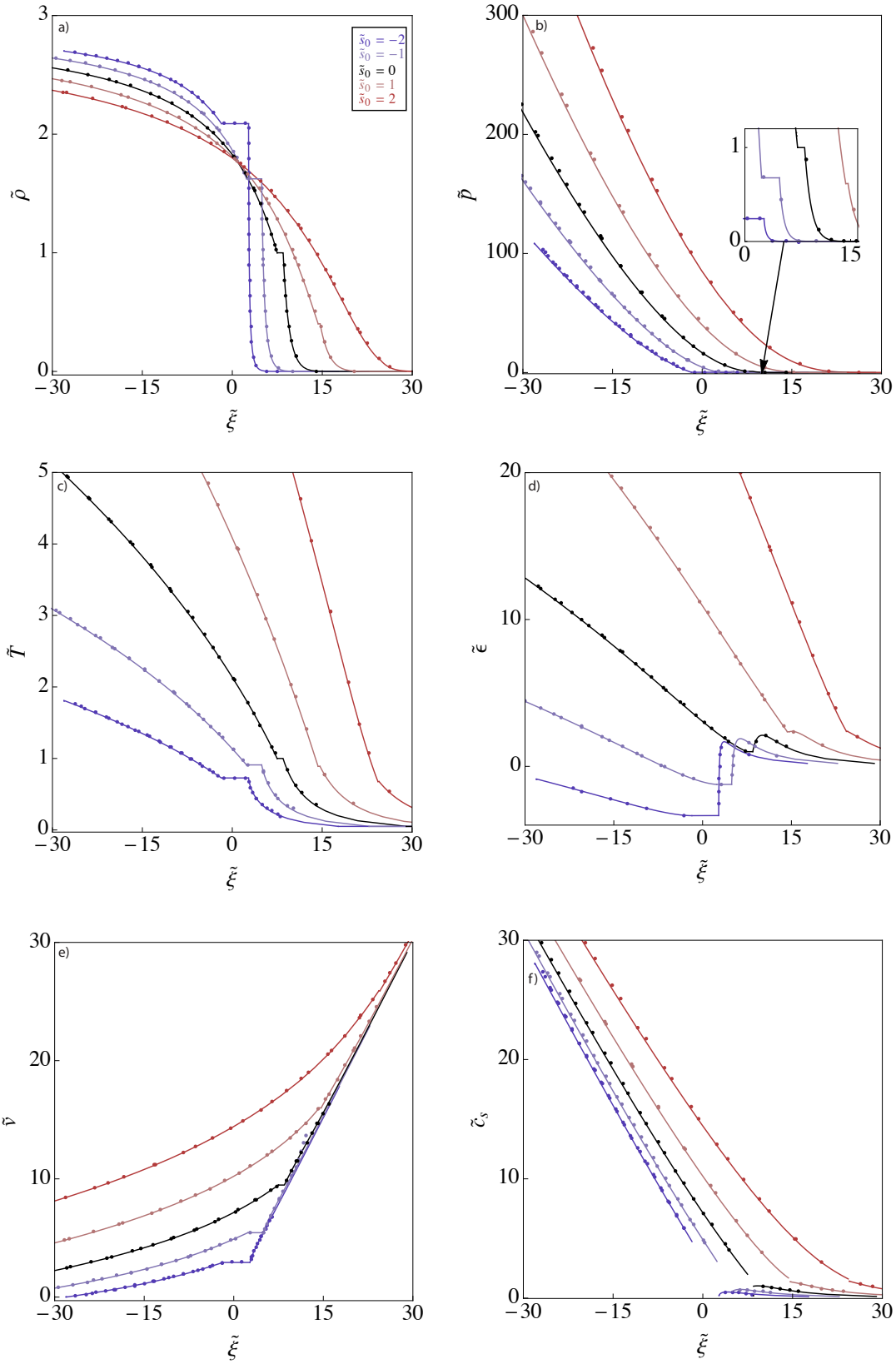

FIG. 2. (Color online) The isentropes from Fig. 1 are represented and follow the same color notation: As a function of $\tilde{\xi}$, (a) fluid density profile $\tilde{\rho}$, (b) fluid pressure profile $\tilde{p}$, (c) fluid temperature profile $\tilde{T}$, (d) fluid energy density profile $\tilde{\epsilon}$, (e) fluid velocity profile $\tilde{v}$ and (f) fluid sound speed profile $\tilde{c}_s$ (note the discontinuity of the sound speed at the binodal). In each plot, an initial density $\tilde{\rho}_0 = 2.7$ is assumed for practical reasons, but each curve can in principle be extended to the left, reaching an asymptotic value of 3. The dots represent the numerical calculations using the 1D planar Lagrangian hydrodynamic code DISH. A expanded representation of this figure can be found in Fig. 3

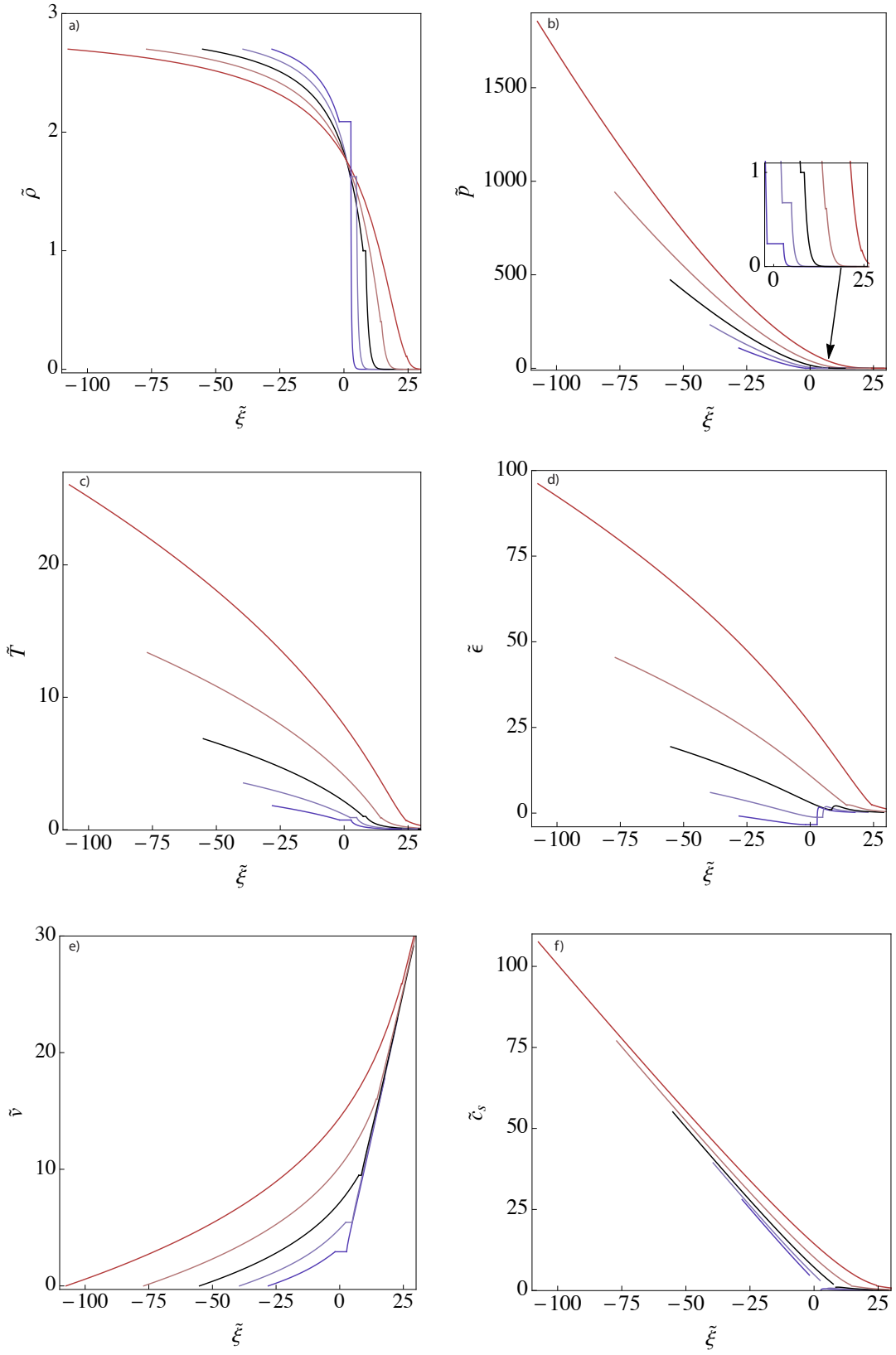

FIG. 3. (Color online) Expanded representation of Fig. 2. The dots are removed for clarity.

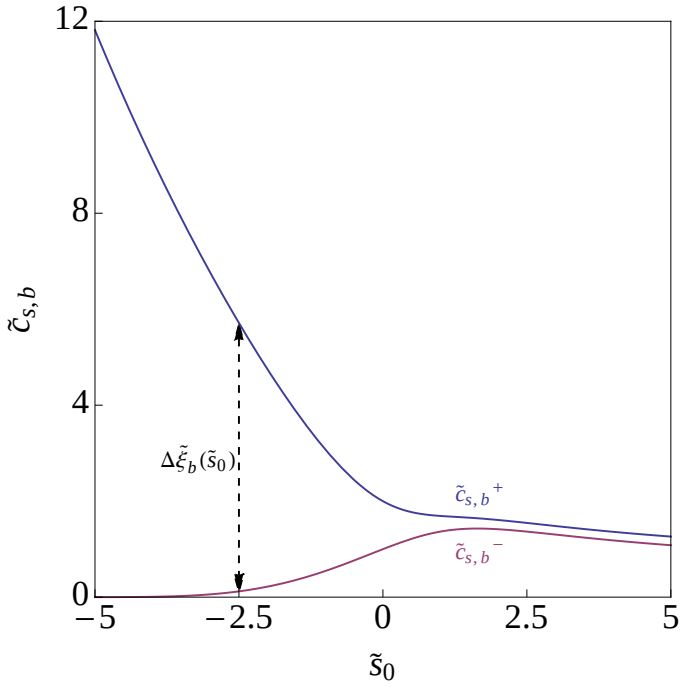

FIG. 4. (Color online) Sound speed $\tilde{c}_{s,b}$ at the vicinity of the binodal as a function of entropy $\tilde{s}_0$: $\tilde{c}^+_{s,b}$ in the single-phase regime, $\tilde{c}^-_{s,b}$ in the two-phase regime. The discontinuity of $\tilde{c}_{s,b}$ yields the length in $\tilde{\xi}$ of the plateau, denoted $\Delta\tilde{\xi}_b$ (see Fig. 5.f).

and by UC Berkeley under Grant DE-FG02-04ER41289. This material is supported by the U.S. D.O.E., Office of Science, Fusion Energy Sciences.

Appendix A: ALGORITHM DETERMINING THE CRITICAL AND INITIAL PARAMETERS

We developed an algorithm to determine the critical and initial parameters (three unknowns: ρ_c, T_c and T_0) from the measurement of four quantities (ρ_0, ρ_b, the length in $\tilde{\xi}$ of the plateau at the binodal $\Delta\xi_b$, the length of the fluid in the dense single phase $\Delta\xi_d$) obtained from a single density profile $\rho(z)$ at a certain time t of an isentropically expanding fluid of known mass number A. Measurement of multiple profiles provides a redundant check on the applicability of the VDW model to the fluid under investigation and/or better accuracy in the unknowns to be determined. Similar algorithm can be easily developed for a single pressure, temperature, energy density or velocity profile.

A density profile $\rho(z)$ for a time t can be readily transformed into a density profile $\rho(\xi)$ of the self-similar variable $\xi = z/t$. From the $\rho(\xi)$ profile, we extract the four input parameters for our algorithm: ρ_0, ρ_b, $\Delta\xi_b = \xi_2 - \xi_1$ and $\Delta\xi_d = \xi_1 - \xi_0$ where $\xi_0 = \xi(\rho_0)$, $\xi_1 = \xi(\rho_b^+)$, $\xi_2 = \xi(\rho_b^-)$.

The density profiles in the (ρ, ξ) plane and in the $(\tilde{\rho}, \tilde{\xi})$ plane differ only by a multiplying factor in ξ and a multiplying factor in ρ such that $\rho = \tilde{\rho}\rho_c$ and $\xi = \tilde{\xi}c_{s,0}$. Those are important features that yield the following properties:

- A given density profile in the (ρ, ξ) plane is associated to a unique dimensionless density profile in the $(\tilde{\rho}, \tilde{\xi})$ plane, and vice versa.
- A point $A(\rho_A, \xi_A)$ in the (ρ, ξ) plane possesses a unique image $\tilde{A}(\tilde{\rho}_{\tilde{A}}, \tilde{\xi}_{\tilde{A}})$ in the $(\tilde{\rho}, \tilde{\xi})$ plane, and vice versa.
- If A, B, C, D are points in the (ρ, ξ) plane, and $\tilde{A}$, $\tilde{B}$, $\tilde{C}$, $\tilde{D}$ their images in the $(\tilde{\rho}, \tilde{\xi})$ plane, the following ratios are conserved: $\frac{\rho_A}{\rho_B} = \frac{\tilde{\rho}_{\tilde{A}}}{\tilde{\rho}_{\tilde{B}}}$ and $\frac{\xi_A - \xi_B}{\xi_C - \xi_D} = \frac{\tilde{\xi}_{\tilde{A}} - \tilde{\xi}_{\tilde{B}}}{\tilde{\xi}_{\tilde{C}} - \tilde{\xi}_{\tilde{D}}}$.

A dimensionless density profile is therefore an image of a dimensional density profile if and only if they have the same ratios

$$R_\rho = \frac{\rho_b}{\rho_0} = \frac{\tilde{\rho}_b}{\tilde{\rho}_0} \text{ and } R_\xi = \frac{\Delta\xi_b}{\Delta\xi_d} = \frac{\Delta\tilde{\xi}_b}{\Delta\tilde{\xi}_d}. \tag{A1}$$

Fig. 5 shows that $\tilde{\rho}_b$ and $\Delta\tilde{\xi}_b$ are functions of only $\tilde{s}_0$, and $\Delta\tilde{\xi}_d$ is a function of only $\tilde{s}_0$ and $\tilde{\rho}_0$. This implies that R_ρ and R_ξ are both functions only of $\tilde{s}_0$ and $\tilde{\rho}_0$. We can therefore trace curves of constant R_ξ and R_ρ in the $(\tilde{\rho}_0, \tilde{s}_0)$ space as shown in Fig. 6.

The algorithm decomposes into seven steps:

1. Fetch one (ρ, z) profile of hydrodynamical expansion at a given t.
2. Transform the (ρ, z) profile into a (ρ, ξ) profile using the self-similar parameters $\xi = z/t$ and store ρ_0, ρ_b, $\Delta\xi_d$ and $\Delta\xi_b$.
3. Compute the ratios R_ρ and R_ξ.
4. Find $\tilde{\rho}_0$ and $\tilde{s}_0$ at the intersection of the R_ρ and R_ξ curves in the $(\tilde{\rho}_0, \tilde{s}_0)$ diagram (see Fig. 6).
5. Extract $\Delta\tilde{\xi}_b$ from Fig. 5.
6. Compute the critical density
$$\rho_c = \rho_0/\tilde{\rho}_0, \tag{A2}$$
the critical temperature
$$kT_c = \frac{8}{3}\left(\frac{\Delta\xi_b}{\Delta\tilde{\xi}_b}\right)^2 Am_{\text{amu}}. \tag{A3}$$
7. Compute the initial temperature
$$kT_0 = kT_c\left(\frac{2\tilde{\rho}_0}{3 - \tilde{\rho}_0}e^{\tilde{s}_0}\right)^{\frac{2}{3}}. \tag{A4}$$

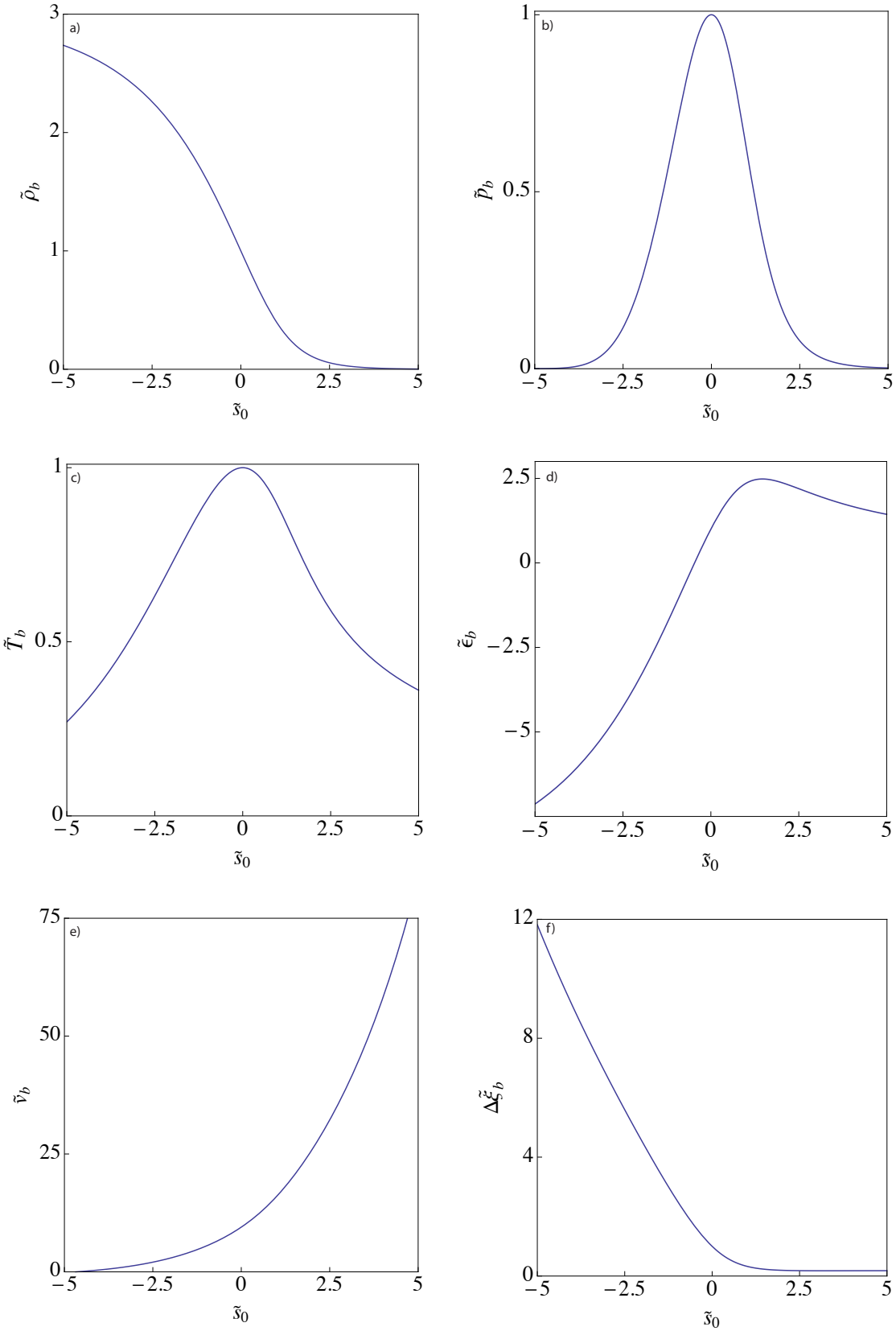

FIG. 5. (Color online) For each value of $\tilde{s}_0$ can be associated at the binodal a unique value of (a) fluid density $\tilde{\rho}_b$, (b) fluid pressure $\tilde{p}_b$, (c) fluid temperature $\tilde{T}_b$, (d) fluid energy density $\tilde{\epsilon}_b$, (e) fluid velocity $\tilde{v}_b$ and (f) plateau in ξ, denoted as $\Delta\tilde{\xi}_b$.

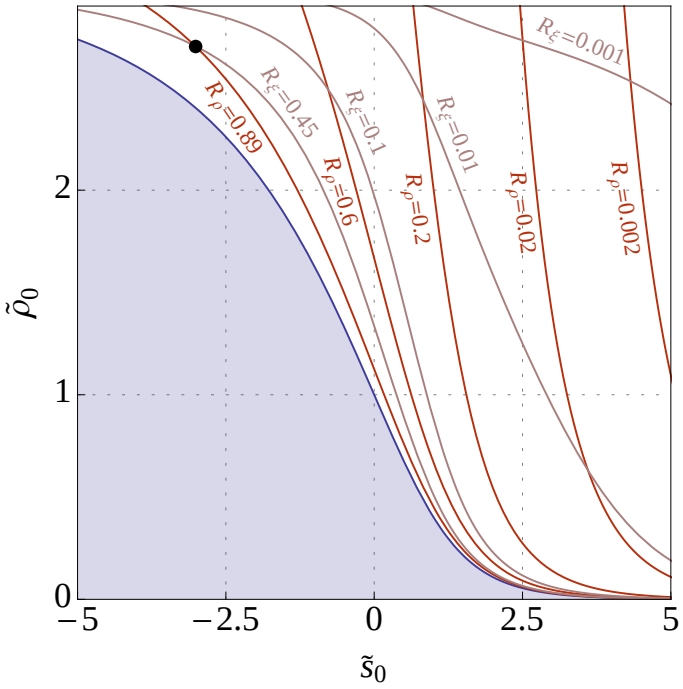

FIG. 6. (Color online) In the $(\tilde{s}_0,\tilde{\rho}_0)$ diagram, we traced the curves of constant ratios $R_\rho = 0.89,\ 0.6,\ 0.2,\ 0.02,\ 0.002$ and $R_\xi = 0.45,\ 0.1,\ 0.01,\ 0.001$. A given R_ρ curve intersects with a given R_ξ curve only once. The blue area is the space where the fluid is already in the two-phase regime at the initial point. The curves $R_\rho = 0.89$ and $R_\xi = 0.45$, found in Appendix B, intersect at $\tilde{s}_0 = -3.01$ and $\tilde{\rho}_0 = 2.70$, represented by the black dot point.

Appendix B: TEST OF THE ALGORITHM

We assume that we are provided a single density profile as in Fig. 7, recorded at $t = 631$ ps after the beginning of the expansion caused by a rarefaction wave. We have generated this profile using the DISH code. We suppose that what is known is that EOS is a standard VDW EOS with the atomic mass number $A = 26.98$.

We can easily transform the $\rho(z)$ profile of Fig. 7 into a $\xi(z)$ profile and we can extract

$$\rho_0 = 2.18 \text{ g.cm}^{-3} \text{ and } \rho_b = 1.93 \text{ g.cm}^{-3} \qquad \text{(B1)}$$

as well as

$$\Delta\xi_b = 7.2\times10^3 \text{ m.s}^{-1} \text{ and } \Delta\xi_d = 1.6\times10^4 \text{ m.s}^{-1}. \qquad \text{(B2)}$$

Their ratios from Eq. (A1) can therefore be readily computed:

$$R_\rho = 0.89 \quad \text{and} \quad R_\xi = 0.45. \qquad \text{(B3)}$$

Using Fig. 6, the corresponding dimensionless density and entropy of the isentropic expansion associated to the rarefaction waves are

$$\tilde{\rho}_0 = 2.70 \text{ and } \tilde{s}_0 = -3.01. \qquad \text{(B4)}$$

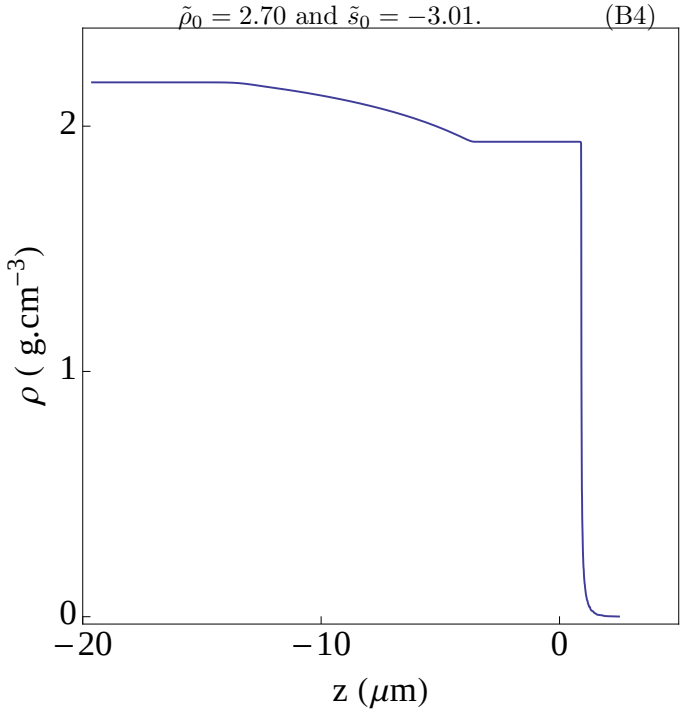

FIG. 7. (Color online) A single density profile generated by the DISH code to test the algorithm of Appendix A. The input parameters are revealed in the end of Appendix B to determine how accurate the algorithm is.

For $\tilde{s}_0 = -3.01$, we extract $\Delta\tilde{\xi} = 6.75$ from Fig. 5, and therefore, Eqs. (A2), (A3) and (A4) yield:

$$\rho_c = 0.80 \text{ g.cm}^{-3}, T_c = 0.87 \text{ eV}, \text{ and } T_0 = 0.81 \text{ eV}. \qquad \text{(B5)}$$

In order to produce Fig. 7 with the DISH code, we entered as input the critical density $\rho_{c,\text{input}} = 0.80$ g.cm^{-3}, the critical temperature $T_{c,\text{input}} = 0.90$ eV and the initial temperature $T_{0,\text{input}} = 0.84$ eV. This represents a negligible error for the density calculations, and an error of 4% or less for the temperature calculations, mostly attributed to finite difference errors in the DISH code when generating Fig. 7.

[1] F. Perrot, M. W. C. Dharma-Wardana, and J. Benage. Possibility of an unequivocal test of different models of the equation of state of aluminum in the coupling regime $\gamma\sim$1-50. *Physical Review E*, 65:046414, Apr 2002.

[2] R. W. Lee, H. A. Baldis, R. C. Cauble, O. L. Landen, J. S. Wark, A. Ng, S. J. Rose, C. Lewis, D. Riley, J.-C. Gauthier, and P. Audebert. Plasma-based studies with intense x-ray and particle beam sources. *Laser and Par-*

ticle Beams, 20:527–536, 7 2002.

[3] M. Koenig, A. Benuzzi-Mounaix, A. Ravasio, T. Vinci, N. Ozaki, S. Lepape, D. Batani, G. Huser, T. Hall, D. Hicks, A. MacKinnon, P. Patel, H. S. Park, T. Boehly, M. Borghesi, S. Kar, and L. Romagnani. Progress in the study of warm dense matter. *Plasma Physics and Controlled Fusion*, 47(12B):B441, 2005.

[4] A. Forsman, A. Ng, G. Chiu, and R. M. More. Interaction of femtosecond laser pulses with ultrathin foils. *Physical Review E*, 58:R1248–R1251, Aug 1998.

[5] D. H. H. Hoffmann, A. Blazevic, O. N. Rosmej, P. Spiller, N. A. Tahir, K. Weyrich, T. Dafni, M. Kuster, M. Roth, S. Udrea, D. Varentsov, J. Jacoby, K. Zioutas, V. Mintsev, V. E. Fortov, B. Yu. Sharkov, and Y. Maron. Frontiers of dense plasma physics with intense ion and laser beams and accelerator technology. *Physica Scripta*, T123(T123):1, 2006.

[6] J. J. Barnard, R. J. Briggs, D. A. Callahan, R. C. Davidson, A. Friedman, L. Grisham, E. P. Lee, R. W. Lee, B. G. Logan, C. L. Olson, D. V. Rose, P. Santhanam, A. M. Sessler, J. W. Staples, M. Tabak, D. R. Welch, J. S. Wurtele, and S. S. Yu. Accelerator and ion beam tradeoffs for studies of warm dense matter. In *Proceedings of the Particle Accelerator Conference, 2005. PAC 2005*, pages 2568–2570, 2005.

[7] F. M. Bieniosek, J. J. Barnard, A. Friedman, E. Henestroza, J. Y. Jung, M. A. Leitner, S. Lidia, B. G. Logan, R. M. More, P. A. Ni, P. K. Roy, P. A. Seidl, and W. L. Waldron. Ion-beam-driven warm dense matter experiments. *Journal of Physics: Conference Series*, 244(3):032028, 2010.

[8] N. A. Tahir, D. H. H. Hoffmann, A. Kozyreva, A. Shutov, J. A. Maruhn, U. Neuner, A. Tauschwitz, P. Spiller, and R. Bock. Equation-of-state properties of high-energy-density matter using intense heavy ion beams with an annular focal spot. *Physical Review E*, 62:1224–1233, Jul 2000.

[9] A. D. Rakhel, A. Kloss, and H. Hess. On the critical point of tungsten. *International Journal of Thermophysics*, 23(5):1369–1380, 2002.

[10] D. von der Linde, K. Sokolowski-Tinten, and J. Bialkowski. Laser-solid interaction in the femtosecond time regime. *Applied Surface Science*, 109-110(0):1 – 10, 1997.

[11] K. Sokolowski-Tinten, J. Bialkowski, A. Cavalleri, D. von der Linde, A. Oparin, J. Meyer-ter-Vehn, and S. I. Anisimov. Transient states of matter during short pulse laser ablation. *Physical Review Lett.*, 81:224–227, Jul 1998.

[12] S. I. Anisimov, N. A. Inogamov, A. M. Oparin, B. Rethfeld, T. Yabe, M. Ogawa, and V. E. Fortov. Pulsed laser evaporation: equation-of-state effects. *Applied Physics A: Materials Science & Processing*, 69:617–620, 1999.

[13] N. A. Inogamov, Yu. V. Petrov, S. I. Anisimov, A. M. Oparin, N. V. Shaposhnikov, D. von der Linde, and J. Meyer-ter-Vehn. Expansion of matter heated by an ultrashort laser pulse. *Journal of Experimental and Theoretical Physics Letters*, 69(4):310–316, 1999.

[14] V.V. Zhakhovskii, K. Nishihara, S.I. Anisimov, and N.A. Inogamov. Molecular-dynamics simulation of rarefaction waves in media that can undergo phase transitions. *Journal of Experimental and Theoretical Physics Letters*, 71(4):167–172, 2000.

[15] J. J. Barnard, J. Armijo, R. M. More, A. Friedman, I. Kaganovich, B. G. Logan, M. M. Marinak, G. E. Penn, A. B. Sefkow, R. Santhanam, P. Stoltz, S. Veitzer, and J. S. Wurtele. Theory and simulation of warm dense matter targets. *Nuclear Instruments and Methods in Physics Research A*, 577:275–283, jul 2007.

[16] A. Yuen and J. J. Barnard. Rarefaction waves in van der waals fluids with an arbitrary number of degrees of freedom. *Physical Review E*, 92:033019, Sep 2015.

[17] G. F. B. Riemann. Ueber die fortpanzung ebener luftwellen von endlicher schwingungsweite. *Abhandlungen der Koeniglichen Gesellschaft der Wissenschaften zu Goettingen*, 8, 1860.

[18] Y. B. Zeldovich and Y. P. Raizer. *Physics of Shock Waves and High-Temperature Hydrodynamic Phenomena*. Dover Publications, 1962.

[19] L. D. Landau and E. M. Lifshitz. *Fluid Mechanics*. Butterworth-Heinemann, 1987.

[20] D. Chandler, J. D. Weeks, and H. C. Andersen. Van der waals picture of liquids, solids, and phase transformations. *Science*, 220(4599):787–794, 1983.

[21] N. M. Bulgakova, I. M. Bourakov, and N. A. Bulgakova. Rarefaction shock wave: Formation under short pulse laser ablation of solids. *Physical Review E*, 63:046311, Mar 2001.

[22] N. M. Bulgakova and I. M. Burakov. Nonlinear hydrodynamic waves: Effects of the equation of state. *Physical Review E*, 70:036303, Sep 2004.

[23] E. Startsev, I. Kaganovich, and R.C. Davidson. Rarefaction shock waves as diagnostic of critical points. In *Workshop on High Power Lasers, SLAC*, October 1-2, 2013.

[24] R. M. More, DISH user manual, LBNL Report, August 2007.

[25] J. D. Van Der Waals. The equation of state for gases and liquids. In *Nobel Lectures in Physics 1*, 1910.

[26] T. L. Hill. *An Introduction to Statistical Thermodynamics*. Dover Publications, 1987.

[27] D. R. Lide. *Handbook of chemistry and physics*. CRC-Press, 93rd edition, 2012.

[28] C. Kittel. *Elementary Statistical Physics*. Dover Publications, 2004.

[29] S. Wolfram. *The MATHEMATICA® Book, Version 4*. Cambridge university press, 1999.

[30] M. E. Foord, D. B. Reisman, and P. T. Springer. Determining the equation-of-state isentrope in an isochoric heated plasma. *Review of Scientific Instruments*, 75(8):2586–2589, 2004.